Environmental Science & Technology

Subscriber access provided by King Abdullah University of Science and Technology Library

Energy and the Environment

Evaluation of electrode and solution area-based resistances enables quantitative comparisons of factors impacting microbial fuel cell performance

Ruggero Rossi, Benjamin P Cario, Carlo Santoro, Wulin Yang, Pascal E. Saikaly, and Bruce E. Logan

Environ. Sci. Technol., **Just Accepted Manuscript** • DOI: 10.1021/acs.est.8b06004 • Publication Date (Web): 27 Feb 2019

Downloaded from http://pubs.acs.org on March 8, 2019

Just Accepted

"Just Accepted" manuscripts have been peer-reviewed and accepted for publication. They are posted online prior to technical editing, formatting for publication and author proofing. The American Chemical Society provides "Just Accepted" as a service to the research community to expedite the dissemination of scientific material as soon as possible after acceptance. "Just Accepted" manuscripts appear in full in PDF format accompanied by an HTML abstract. "Just Accepted" manuscripts have been fully peer reviewed, but should not be considered the official version of record. They are citable by the Digital Object Identifier (DOI®). "Just Accepted" is an optional service offered to authors. Therefore, the "Just Accepted" Web site may not include all articles that will be published in the journal. After a manuscript is technically edited and formatted, it will be removed from the "Just Accepted" Web site and published as an ASAP article. Note that technical editing may introduce minor changes to the manuscript text and/or graphics which could affect content, and all legal disclaimers and ethical guidelines that apply to the journal pertain. ACS cannot be held responsible for errors or consequences arising from the use of information contained in these "Just Accepted" manuscripts.

ACS Publications

is published by the American Chemical Society. 1155 Sixteenth Street N.W., Washington, DC 20036

Published by American Chemical Society. Copyright © American Chemical Society. However, no copyright claim is made to original U.S. Government works, or works produced by employees of any Commonwealth realm Crown government in the course of their duties.

Evaluation of electrode and solution area-based resistances enables quantitative comparisons of factors impacting microbial fuel cell performance

Ruggero Rossi[1], Benjamin P. Cario[1], Carlo Santoro[2], Wulin Yang[1], Pascal Saikaly[3], Bruce E. Logan[1]*

[1]Department of Civil and Environmental Engineering, The Pennsylvania State University, 231Q Sackett Building, University Park, PA 16802, USA

[2] Department of Chemical and Biological Engineering, Center for Micro-Engineered Materials (CMEM), University of New Mexico, Advanced Materials Lab, 1001 University Blvd. SE Suite 103, MSC 04 2790, Albuquerque, NM 87131, USA.

[3]Biological and Environmental Sciences and Engineering Division, Water Desalination and Reuse Research Center, King Abdullah University of Science and Technology, Thuwal, 23955-6900, Saudi Arabia

*Corresponding author: e-mail: blogan@psu.edu; phone: +1-814-863-7908; fax: +1-814-863-7304

ABSTRACT

Direct comparisons of microbial fuel cells (MFCs) based on maximum power densities are hindered by different reactor and electrode sizes, solution conductivities, and materials. We propose an alternative method here, the electrode potential slope (EPS) analysis, to enable quantitative comparisons based on anode and cathode area-based resistances and operating potentials. Using the EPS analysis, the brush anode resistance (R_{An}= 10.6 ± 0.5 mΩ m^2) was shown to be 28% less than the resistance of a 70% porosity diffusion layer (70% DL) cathode (R_{cat} = 14.8 ± 0.9 mΩ m^2), and 24% less than the solution resistance (R_{Ω} = 14 mΩ m^2) (acetate in 50 mM phosphate buffer solution). Using a less porous cathode (30% DL) did not impact the cathode resistance, but it reduced the cathode performance due to a lower operating potential. With low conductivity domestic wastewater (R_{Ω} = 87 mΩ m^2), both electrodes had higher resistances, with R_{An} = 75 ± 9 mΩ m^2 and R_{Cat} = 54 ± 7 mΩ m^2 (70% DL). Our analysis of the literature using the EPS analysis shows how electrode resistances can easily be quantified to compare system performance when the electrode distances are changed or the electrodes have different sizes.

Introduction

Microbial fuel cells (MFCs) use bacteria on the anode to produce an electrical current from the degradation of organic matter, and a catalyst on the cathode for the oxygen reduction reaction (ORR).[1–4] Many different anode materials have been examined, including graphite fiber brushes, carbon veils, carbon cloth, carbon paper and carbon felt, and these materials have often been modified to increase power production.[5–8] The materials and catalysts used for the cathode have also varied, with the most common types consisting of Pt catalysts on carbon cloth, or activated carbon as both the supporting material and catalyst.[9,10] Typically, improved performance by electrode modification is demonstrated based on an increase in the maximum power production using polarization data.[11,12] However, when a new anode or cathode material is shown to improve performance in one type of MFC, it is not clear how much that specific change improved performance relative to other differences in reactor design, construction, or operational procedures. For example, the power production can be a function of the size (e.g. projected area) of the electrode, as the power per area can vary inversely with electrode size.[13–15] Power is also affected by the relative sizes of the two electrodes (e.g. a larger anode than the cathode).[16] Comparisons of performance are particularly difficult for systems that have different distances between the electrodes, as ohmic resistance can greatly limit overall performance in low conductivity solutions, such as domestic wastewater.[17] Even when all materials and solutions are kept constant, maximum power densities obtained in the same laboratory can vary by ~15%.[9]

In order to better engineer large-scale MFCs, it is necessary to know what specific factors limit performance, and how the behavior of the electrodes will change as they become larger or distances change between them.[18] As the system scale is increased, the performance of one electrode, for example the cathode, could change at a rate with size that is different from that of the anode. As a result, reporting the change in maximum power density alone does not provide insight into which

electrode might be limiting performance, or to what extent, electrode performance changes with reactor size. It is possible to examine abiotic electrode performance using electrochemical techniques such as potentiodynamic (linear sweep voltammetry (LSV)) or potentiostatic methods (chronoamperometry at defined potentials).[19–22] However, these electrochemical techniques cannot be conducted on the anode before it is fully acclimated in an MFC. Also, evaluating anode performance is more difficult than that of an abiotic cathode as its performance can change over time as a function of its operating conditions (e.g. potential, external resistance, temperature).[23–25] Thus, anode performance can only be assessed during actual MFC operation using polarization data and reference electrodes. However, the ohmic drop between the reference and working electrodes must be included in the final polarization data in order to properly evaluate electrode performance as a function of current.[17,26] Inaccurate electrode potentials can lead to wrong conclusions about the extent that the anode or cathode could be limiting power production.[17]

A new and more comprehensive analysis was used here to provide quantitative comparisons of electrodes in different types of MFCs. The slopes of electrode polarization data near peak power, based on the linear region, were used to quantify electrode area-based resistances (mΩ m^2), and the *y*-intercepts of the data were used to calculate effective half-cell potentials. While these factors have been included to some degree in previous studies,[16,27,28] our electrode potential slope (EPS) analysis is unique in terms of the comprehensive nature of the analysis and full use of linearized electrode potential data. In the conventional fuel cell literature, most polarization data have three regions: an initial rapid change in potential at low current densities where the activation losses prevail over the other resistances; a linear region dominated by the ohmic resistances; and a steep decrease in voltage at high current due to mass transfer limitations.[29–32] In MFCs, polarization data are usually linear over a wide range of relevant current densities (especially near the peak power).[16] Anode potentials are linear until very high current densities are reached, where current production can suddenly fail to increase for a variety of reasons

(e.g. substrate limited mass transport, insufficient acclimation or limiting current densities), causing the power curve to exhibit power overshoot (a doubling back of the power curve).[33,34] Cathode potentials typically have an initial rapid drop due to the activation losses of the ORR at low current densities. After this initial drop, the cathode potential tend to be linear at higher current densities (and near peak power production). The slopes of polarization curve for the whole cell, or for individual electrodes, can therefore be used to obtain area-normalized resistances, with the *y*-intercepts of the potentials providing a useful estimate of the actual working open circuit voltages (OCVs).[35] The utility of the EPS analysis method was demonstrated here in experiments using MFCs with brush anodes and cathodes with diffusion layers (DLs) that had two different porosities (70% and 30%), in tests with an acetate-buffered medium and with domestic wastewater. Additionally, this approach was shown to be broadly applicable by evaluating data from previous studies and making quantitative comparisons between electrodes of different size or material. These comparisons demonstrate that it was possible to easily quantify how the specific changes in electrodes or materials affects power production for different types of MFCs.

Materials and methods

Calculations. The overall cell potential (E_{cell}) with a load on the circuit is usually expressed as a function of the electromotive force (E_{emf}) calculated from the anode and cathode half-cell potentials (E_{An} and E_{Cat}), and resistances (R) in the circuit as:[17]

$$E_{cell} = E_{emf} - (\sum \eta_{An} + |\sum \eta_{Cat}| + R_{\Omega}\, i) \quad (1)$$

where η_{An} is the anode overpotential, η_{Cat} the cathode overpotential, R_{Ω} the ohmic resistance, and i the current. Although not explicitly shown in these equations, the electrode overpotentials are a function of the current, and thus they decrease the voltage due to activation losses, pH changes, bacterial metabolic losses, and concentration losses (mass transfer limitations to or from the electrodes). To account for

different sizes of electrodes, current density (A m^{-2}) is used based on the electrode projected area, and therefore the resistance must also have units of area (mΩ m^2) for a given voltage (mV).[28]

The theoretical E_{emf} can be calculated from the half-cell reactions, chemical activities, and operational conditions. Eq. 1 can be written in terms of the half-cell potentials for the anode (E_{An}) and cathode (E_{Cat}) as

$$E_{cell} = E_{Cat} - E_{An} - (\sum \eta_{An} + |\sum \eta_{Cat}| + R_{\Omega}\, i) \quad (2)$$

The typical electrochemical reactions of an MFC are acetate oxidation at pH 7 at the anode[1] and oxygen reduction at the cathode. Assuming acetate oxidation produces bicarbonate, and assuming the ORR occurs with a $4e^-$ transfer proceeds through either proton uptake or water dissolution,[36,37] possible reactions and half cell potentials (25 °C and pH=7) are:

$$2HCO_3^- + 8e^- + 9H^+ \rightleftharpoons CH_3COO^- + 4H_2O \qquad E_{An} = -296 \text{ mV} \qquad (3)[1]$$

$$O_2 + 4e^- + 2H_2O \rightleftharpoons 4OH^- \qquad E_{Cat} = +815 \text{ mV} \qquad (4a)$$

$$O_2 + 4e^- + 4H^+ \rightleftharpoons 2H_2O \qquad E_{Cat} = +815 \text{ mV} \qquad (4b)$$

where the half-cell potentials are given versus a standard hydrogen electrode (SHE). This results in theoretical values of E_{emf} = 1111 mV. However, for activated carbon (AC) electrodes, oxygen reduction can also proceed through a $2e^-$ transfer mechanisms,

$$O_2 + 2e^- + 2H^+ \rightleftharpoons H_2O_2 \qquad E_{Cat} = +281 \text{ mV} \qquad (5)$$

$$O_2 + 2e^- + 2H_2O \rightleftharpoons H_2O_2 + 2OH^- \qquad E_{Cat} = +267 \text{ mV} \qquad (6)$$

$$O_2 + 2e^- + H_2O \rightleftharpoons HO_2^- + OH^- \qquad E_{Cat} = +337 \text{ mV} \qquad (7)$$

resulting in a range of electrons transferred between 2.1 – 3.6 e^-.[11,38,39] Thus, the measured E_{emf} ($E_{emf,m}$) for the cell, for example at open circuit conditions ($E_{emf,m0}$), does not have a single predictable value due to the multiple ORRs.

The measured cell voltage can rapidly decrease at low current densities due to activation losses and other changes that impact the operational conditions near the electrode, such as localized pH that can switch electron transfer mechanism pathway or carbonate concentrations that become different than the bulk phase concentrations. Following this rapid decline in voltage, the electrode potentials become a linear function of current. For operation past these low current densities, the electrode potentials in eq. 2 can be replaced by potentials fit to the linear portion of the measured anode and cathode potentials, producing operational potentials that better describe the working electrode potentials in terms of experimental electrode potentials conditions, for the anode ($E_{An,e0}$) and cathode ($E_{Cat,e0}$) potentials. Since all changes in electrode and solution potentials are now a linear function of the current, eq. 2 can now be written as

$$E_{cell} = E_{Cat,\,e0} - E_{An,e0} - i(R_{Cat} + R_{An} + R_{\Omega}) \quad (8)$$

where the electrode overpotentials that impact the measured cell voltage are quantified in terms of individual resistances of the anode (R_{An}), cathode (R_{Cat}), and electrolyte (R_{Ω}). If a membrane or separator is used, resistances for these materials would be included in a measured R_{Ω}, or they would need to be separately determined from the electrolyte resistance. The sum of these three resistances in eq. 8 is the total operational internal resistance (R_{int}).

To evaluate the performance of an MFC, the load on the circuit is typically varied by using an external resistance, and the operational current is calculated from the cell voltage. Thus, we can replace E_{cell} with the external resistance in the circuit (R_{ext}) as a function of the current, as

$$iR_{ext} = E_{Cat,\,e0} - E_{An,e0} - i(R_{Cat} + R_{An} + R_{\Omega}) \quad (9)$$

Based on eq. 9, a circuit can be drawn that describes the steady performance of the cell (i.e. neglecting sudden changes in the load on the circuit) (Figure 1A). For this EPS analysis of the electrode open circuit potentials and resistances, the electrode potentials were obtained from the polarization test by

changing the external resistance in the circuit. The electrode potentials are then plotted with the potential on the y-axis, and the current density on the x-axis. The linear portion of the data are expressed as $E = m\,i + b$, where the slope m is the specific resistance of each electrode (R_{Cat} or R_{an}) in units of mΩ m^2, and the y-intercepts are used to calculate the experimental open circuit potentials of the anode ($E_{An,e0}$) or cathode ($E_{Cat,e0}$) (Figure 1B). The solution resistance, R_Ω (mΩ m^2), can be obtained from the solution conductivity (σ, mS cm^{-1}), and the distance between the electrodes (l, cm), as

$$R_\Omega = \frac{100\ l}{\sigma} \tag{10}$$

where 100 is used for unit conversion (conversion of mS into S, where 1 S = 1 Ω^{-1}, and cm^2 to m^2). For example, for 50 mM PBS (σ = 6.9 mS cm^{-1}) and an electrode spacing of l = 1 cm, R_Ω = 14 mΩ m^2. If a membrane or separator is used, electrochemical impedance spectroscopy (EIS) can be used to obtain the membrane resistance from the combined solution and membrane resistance.[40]

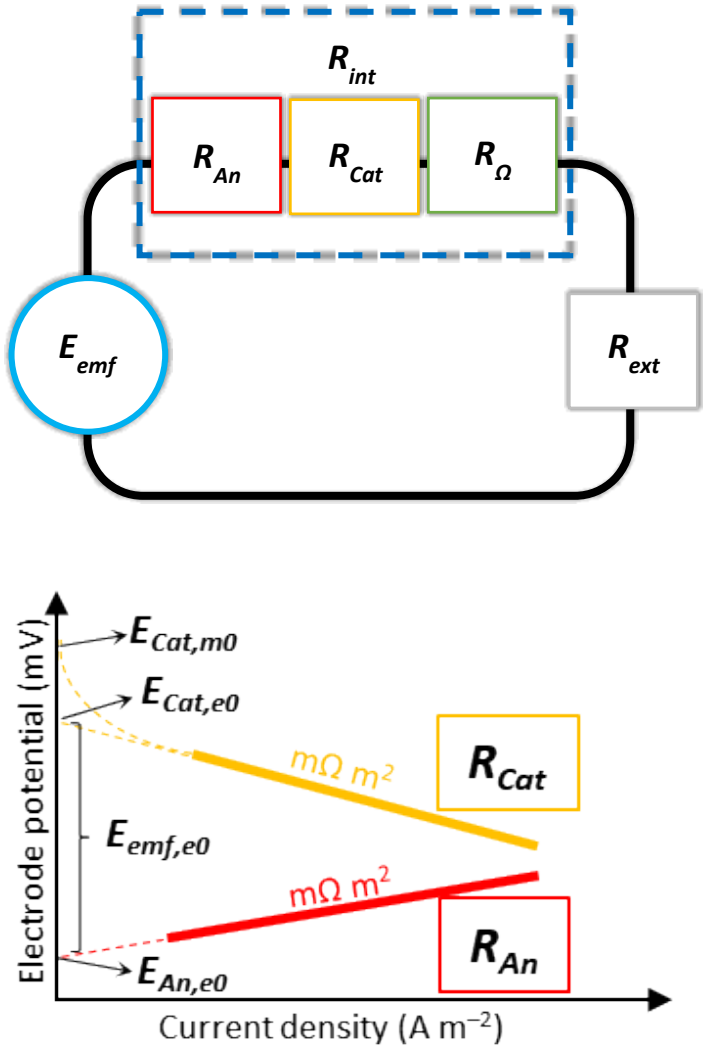

Figure 1. (A) Microbial fuel cell circuit diagram with anode, cathode and ohmic resistances as part of the total internal resistance of the cell. The membrane resistance was not inserted in the figure as no membrane is currently used in single chamber MFCs. (B) Schematic representation of the parameters used for the EPS analysis. The dashed lines represent the linearization that would be obtained from polarization tests, while the thick solid lines show the linearized portion of the polarization data that are used to calculate the anode (R_{An}) and cathode (R_{Cat}) resistances.

The above EPS analysis, based on using the slopes and *y*-intercepts of the polarization data to measure electrode resistances and calculate working half-cell potentials, is different from previous approaches that used area-based electrode resistances. For example, Fan et al. (2008) did not directly measure each electrode resistances and instead used only whole cell polarization data.[16] This method

resulted in errors in calculated electrode resistances, as they were assumed to be constant with changes in conductivity. Sleutels et al. (2009) calculated electrode resistances for MECs using a single condition (i.e. one point for each resistance calculated) rather than using many points (i.e. the linearized portion of the polarization data) which reduced accuracy, and theoretical half-cell potentials rather than those obtained from the *y*-intercept as done here.[28] Liang et al. calculated resistances using a slope analysis of the polarization data, but they also did not use *y*-intercepts to calculate the experimental electrode potentials, nor did they consistently correct electrode polarization data for ohmic losses or calculate solution resistances from solution conductivities.[27] Instead, the current interrupt method was used to estimate ohmic losses.

Construction and operation of MFCs. MFCs contained 28 mL (empty volume) cylindrical chambers cut into polycarbonate blocks, with a chamber 3 cm in diameter and 4 cm in length.[9] The anodes were carbon brushes 2.5 cm in diameter, and 2.5 cm long, which were made by twisting conductive carbon fibers between two titanium wires.[5] All brushes were heat treated at 450 °C for 30 min in a muffle furnace prior to use.[41] Anodes were acclimated in MFCs for over two years at a fixed external resistance of 1000 Ω, at a constant temperature (30 °C) prior to use here with new cathodes. Cathodes (7 cm^2 exposed surface) were made from activated carbon (AC) and stainless steel mesh, with a cathode specific surface area per volume of reactor of 25 m^2 m^{-3}.[2] AC cathodes were manufactured by VITO (Mol, Belgium), and had diffusion layers (DLs) with different porosities of 70% or 30% in order to study two different types of cathodes.[42] Anode and cathode specific resistances were normalized by the cathode projected area (7 cm^2).

Brush anodes were placed near the cathode (electrode spacing of $d_{An\text{-}Cat}$ = 1 cm in phosphate buffer and $d_{An\text{-}Cat}$ = 1.3 cm in wastewater tests) with the brush perpendicular to the cathode and the reference electrode (RE) tip touching the titanium wire. The larger spacing used in the wastewater tests was set to

match that of a larger-scale MFC, where this distance was chosen to minimize possible clogging with domestic wastewaters.[7] The REs used to measure electrode potentials (Ag/AgCl; model RE-5B, BASi, IN; +0.209 V versus a standard hydrogen electrode, SHE) were placed in the current path between the electrodes. The RE was 0.5 cm in diameter, with a tip diameter of 0.4 cm. Distances between electrodes are considered to be accurate to within 0.2 cm. All potentials are reported here versus SHE.

Tests were conducted using a medium containing a 50 mM phosphate buffer solution (PBS; 4.58 g Na_2HPO_4, 2.45 g NaH_2PO_4, 0.31 g NH_4Cl, 0.13 g KCl in 1 L of distilled water, with 12.5 mL of a concentrated trace mineral solution and 5 mL of a vitamin solution) amended with sodium acetate (1 g/L) having a conductivity of 6.93 mS cm^{-1}, or domestic wastewater (WW).[43] Wastewater was collected weekly from the primary clarifier of the Pennsylvania State University Waste Water Treatment Plant, and stored at 4 °C prior to use. Solution conductivity of the wastewater was 1.51 mS cm^{-1} at 25 °C. The MFCs were operated at 30 °C in a controlled temperature room.

Electrochemical measurements. MFCs were acclimated as previously described,[44] based on feeding the reactor with media in fed-batch operation over several weeks, until at least 3 reproducible and stable voltage profiles were obtained. Single cycle polarization tests were conducted by feeding the reactor with fresh media and maintaining the system at open circuit conditions for 2 h, and then steadily reducing the external resistance from 1000, 500, 200, 100, 75, 50 to 25 Ω at 20 min intervals. Polarization tests were completed before there was an appreciable change in the pH or substrate concentrations that could impact performance.

The current was calculated based on the potential (E_{cell}) measured across the external resistor, and recorded using a computer based data acquisition system (2700, Keithley Instrument, OH). Current densities (i) and power densities (P) were normalized to the total exposed cathode area (A = 7 cm^2) and calculated as $i = E_{cell}/R_{ext}A$ and $P = iE_{cell}$, where R_{ext} is the external resistance.[44]

During each polarization test, the electrode potentials were recorded using a reference electrode. The RE was used to measure the anode potential (E_{An}), the cathode potential (E_{Ct}) was then calculated from the anode potential and the whole cell voltage as $E_{Ct} = U + E_{An}$. The electrode potential was then corrected based on the conductivity of the solution (~1.5 mS cm^{-1} for the wastewater and 6.9 mS cm^{-1} for the PBS) and the distance from each electrode to the RE by rearranging eq. 10 and dividing R_Ω by the projected area of the electrode.[17] The measured electrode potentials (not corrected for the solution conductivity) are reported in the Supporting Information.

Results and discussion

Experimental whole cell polarization curves in PBS and wastewater. The measured total cell open circuit potential was $E_{emf,m0}$ = 664 ± 11 mV for the 70 % DL cathode MFCs fed acetate in PBS, similar to that for the 30% DL (669 ± 4 mV) (Figure 2 A,B). These values were both ~40% lower than the theoretical E_{emf} = 1111 mV, assuming a 4e$^-$ transfer at pH=7.[36] The experimental potential of the 70% DL cathode MFC was $E_{emf,e0}$ = 531 ± 5 mV, based on the *y*-intercept of the cell polarization data (current density range of 3 – 9 A m^{-2}). When using the less porous 30% DL, the experimental potential was reduced to an $E_{emf,e0}$ = 467 ± 22 mV, suggesting that the less porous DL reduced the maximum working potential of the MFC.

The maximum measured power density was 1.71 ± 0.08 W m^{-2} for the 70% DL, and 1.38 ± 0.04 W m^{-2} for the 30% DL, consistent with previous reports on improved performance with a more porous DL.[42] The internal resistances obtained from the linearized polarization data for these MFCs with the two different cathodes, however, were quite similar: 41 ± 1 mΩ m^2 (70% porosity), and 39 ± 4 mΩ m^2 (30% DL). The similar area-specific resistances suggests that the lower power density with the cathode with 30% DL was due to a decrease in the $E_{emf,e0}$ of more than 60 mV compared to the 70% DL, and not to differences in electrode resistances. However, this requires measurement of electrode potentials, as

248 shown below. Using the circuit shown in Figure 1, and the experimental potentials and total specific
249 resistances (obtained from the lines), the calculated maximum power densities were 1.71 W m^{-2} (70%
250 porosity) and 1.40 W m^{-2} (30% porosity), showing good agreement with the experimental results (Figure
251 2).
252

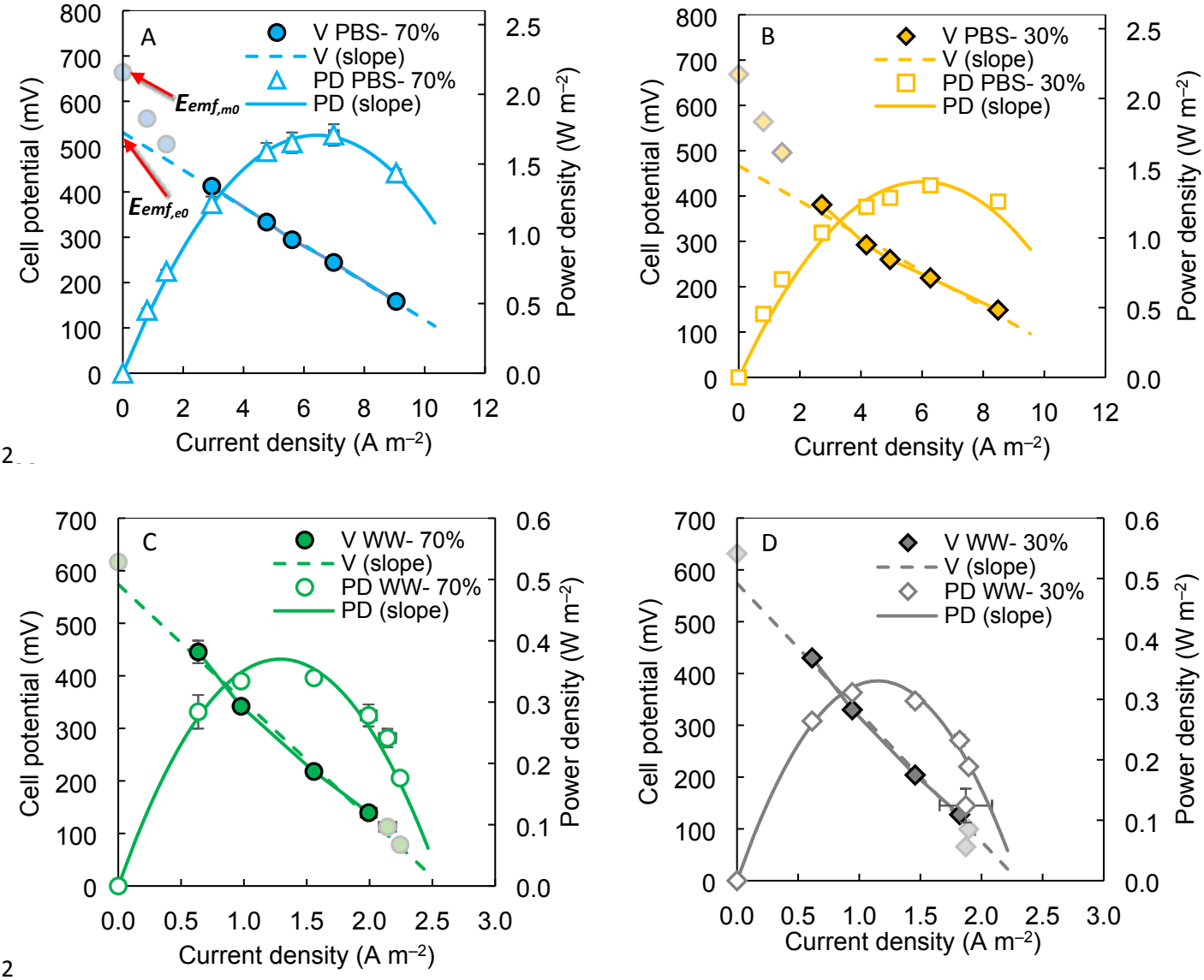

253
254

Figure 2: Modeled polarization and power density curves based on a single internal resistance calculated by the slope of the I-E_{cell} curve and several external resistances compared to the data from polarization test in (A,B) PBS and (C,D) wastewater using cathodes with diffusion layer porosities of 70% (A, C) and

30% (B, D). The dashed lines represent the linearization of the data that would be obtained from polarization tests.

The measured open ciruit whole cell potentials in wastewater of the MFCs with the two different cathodes were $E_{emf,m0}$ = 617 ± 2 mV (70% DL) and $E_{emf,m0}$ = 632 ± 2 mV (30% DL) (Figure 2C, 2D). These potentials were slightly lower than those measured using acetate in PBS, likely reflecting the less thermodynamically favorable oxidation of wastewater organics compared to acetate alone. The experimental $E_{emf,e0}$ were the same for the MFCs with the different cathodes (574 ± 22 mV with 70% DL, and 574 ± 16 mV with 30% DL).

The internal resistance of the MFCs based on the slopes of the polarization data with wastewater was 223 ± 16 mΩ m^2 for the 70% DL, which was only 11% lower than that of the MFCs with the 30% DL (249 ± 12 mΩ m^2). As a result of the similar experimental potentials and internal resistances, the maximum power densities were also quite similar with 0.34 ± 0.01 W m^{-2} (70% DL) and 0.31 ± 0.01 W m^{-2} (30% DL). The ohmic resistance of the wastewater (87 mΩ m^2) was much higher than PBS (14 mΩ m^2). The impact of this large ohmic resistance of the wastewater, coupled with the low current density, likely reduced the impact of the different DL porosities on power production. The maximum power densities calculated from the $E_{emf,e0}$ and the internal resistance in each configuration resulted similar maximum power densities of 0.37 W m^{-2} (70% porosity) and 0.33 W m^{-2} (30% porosity), and were in good agreement with polarization data.

Electrode potentials and specific resistances. The measured cathode potentials at open circuit conditions using acetate and PBS were $E_{Cat,m0}$ = 399 ± 11 mV (70 % DL cathode) and $E_{Cat,m0}$ = 401 ± 2 mV (30 % DL cathode), which were around 400 mV lower than the theoretical value at pH 7 (for example +815 mV using eq. 4b). The experimental cathode potentials with the 70% DL cathode ($E_{Cat,e0}$ = 271 ± 6 mV) was 32% higher than that of the 30% DL cathode ($E_{Cat,e0}$ = 205 ± 27 mV) (Figure 3A), while the area-

specific resistances of the two different cathodes were quite similar (14.8 ± 0.9 mΩ m^2, 70% DL; 12 ± 5 mΩ m^2, 30% DL cathode). The anode potentials did not change when using the different cathodes ($E_{An,e0}$ = –260 ± 3 mV, 70% DL; –262 ± 7 mV, 30% DL), nor did the anode area resistances (10.6 ± 0.5 mΩ m^2, 70% DL; 11 ± 1 mΩ m^2, 30% DL). This conclusively demonstrated that the differences in power production using the two different cathodes was specifically due to the cathode, and not any changes in the anode potentials (for example due to greater oxygen transfer through the higher porosity cathode). The slightly higher resistances for the cathodes than the anodes suggest that the cathode limited power production only slightly more than the anodes.

Using the EPS analysis, the power density curve was accurately reproduced, allowing clear identification of both the individual resistances and the working potentials. The sum of the singular resistances (R_{An}, R_{Cat}, and R_{Ω} = 14 mΩ m^2) from the electrode slopes and solution conductivity was 39.4 mΩ m^2, which was within 4% of that calculated from the slope of the whole cell polarization curve (41 ± 1 mΩ m^2, 70% DL cathode). With the 30% DL cathode, 37 mΩ m^2 was calculated from the sum of the individual resistances compared to 39 ± 4 mΩ m^2 using the whole cell polarization curve. The use of $E_{Cat,e0}$ based on experimental polarization data has the advantage of using most of the polarization data to obtain the working potentials, rather than just a single point as done by Sleutels et al.[28] In studies by others, theoretical or measured open circuit cathode potentials were used,[16,27] which would have resulted in potentials that did not accurately predict MFC performance.

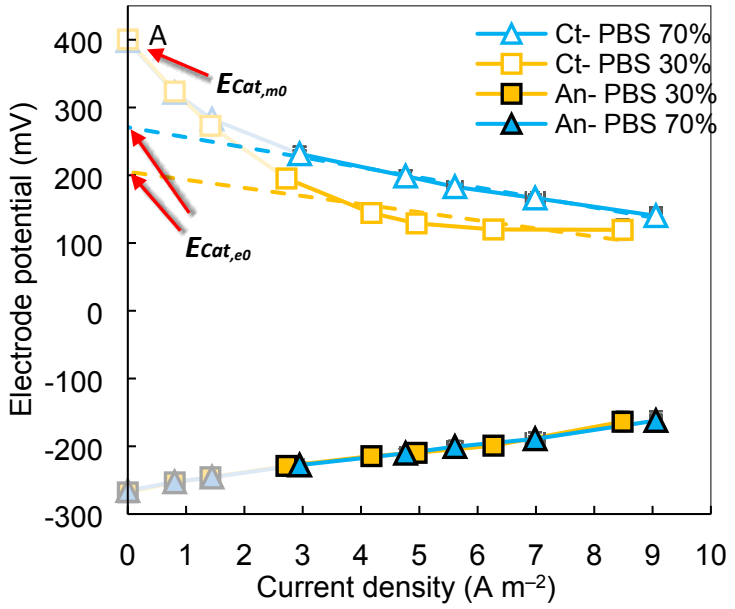

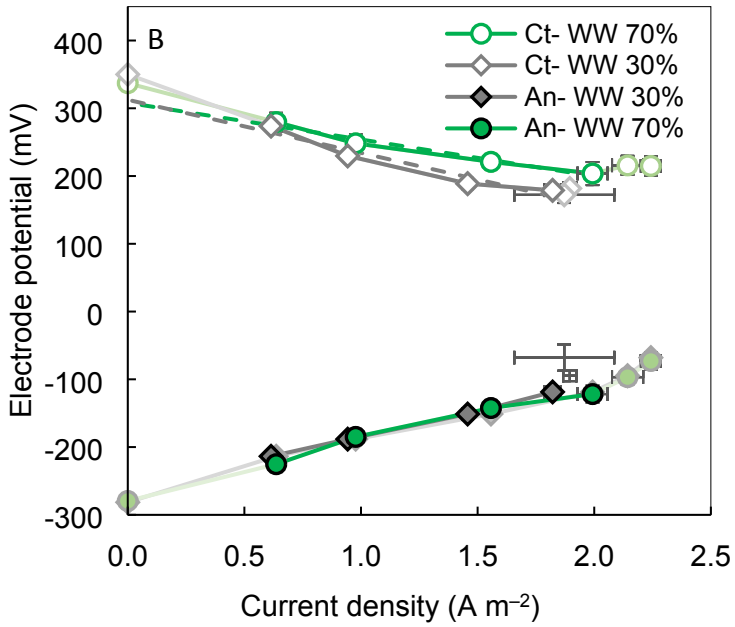

Figure 3. Anode (An) and cathode (Ct) potentials following correction for ohmic resistance in (A) PBS and (B) wastewater using cathodes with 70% or 30% DL porosities. Anode and cathode potentials not corrected for ohmic losses are reported in the Supporting information (Figure S1). The dashed lines represent the linearization of the data that would be obtained from polarization tests, while the thick solid lines show the linearized portion of the slopes that are used to calculate the anode (R_{An}) and cathode (R_{Cat}) resistances.

Using wastewater, the measured cathode potentials of $E_{Cat,m0}$ = 337 ± 1 mV (70 % DL cathode) and 350 ± 2 mV (30 % DL cathode) were slightly higher than those obtained from the slope analysis of $E_{Cat,e0}$ = 308 ± 10 mV (70% DL) and 313 ± 18 mV (30% DL). The measured $E_{Cat,m0}$ and the experimental $E_{Cat,e0}$ cathodes potentials were much similar to each other in wastewater tests, compared to PBS where $E_{Cat,e0}$ differed from $E_{Cat,m0}$ as much as 50% (cathodes with 30% DL). The narrower differences between the experimental and measured E_{Cat} for the wastewater samples could have been due to the low current densities, as this results in operation of the MFC in a region of current that includes activation losses in the final R_{Cat} and $E_{An,e0}$ (see Supporting Information, and Figure S2). The measured anode potentials in wastewater were both $E_{An,m0}$ –280 ± 3 mV, with more positive anode potentials from the slope analysis of $E_{An,e0}$ = –266 ± 13 mV (70% DL) and –262 ± 3 mV (30% DL). These anode potentials were quite similar to the operational potentials obtained using PBS.

The cathode specific resistances R_{Cat} in wastewater were both substantially higher in respect to PBS, with 54 ± 7 mΩ m^2 (70% DL) and 78 ± 14 mΩ m^2 (30% DL). These cathode specific resistances were 4× – 7× higher in wastewater than those obtained in PBS. The anode specific resistances were also greatly increased, with similar resistances obtained of 75 ± 9 mΩ m^2 (70% DL) and 78 ± 2 mΩ m^2 (30% DL). Thus, a 6× increase in the solution specific resistance of the wastewater (R_Ω = 87 mΩ m^2) compared to PBS (R_Ω = 14 mΩ m^2) led to a 4× – 7× higher cathode resistances, and a 7× higher anode resistances, although it did not greatly impact the measured electrode open circuit potentials. The anode and cathode resistances with 30% or 70% DL cathodes were both lower than the solution specific resistance in wastewater, suggesting a large impact of the solution conductivity on the MFC performance. This was different from the case with PBS and acetate where the cathodes primary limited the power production. The sum of the individual area-based resistances were 216 mΩ m^2 (70% DL) and 243 mΩ m^2 (30% DL), both in good agreement (~ 4% less) with the whole cell area specific resistances calculated from the

slopes of the whole cell polarization curves (223 ± 16 mΩ m^2 for the 70% DL and 249 ± 12 mΩ m^2 for the 30% DL).

Comparison of different cathode catalyst and MFC architecture and configurations. The EPS analysis makes it possible to quantify electrode performance and compare the results with other studies and determine how the individual electrode area resistances impacted overall power production. For example, maximum power densities in two studies were reported to be similar, but the EPS analysis shows that this was for different reasons. In one study by Yang et al.,[11] the maximum power density was 2.60 ± 0.05 W m^{-2} using an activated carbon cathode with an Fe-N-C catalyst (28 mL MFC, anode projected area A_{An} = 4.9 cm^2, cathode projected area A_{Cat} = 7 cm^2, and an electrode spacing of $d_{An\text{-}Cat}$ =0.5 cm, and solution conductivity σ = 6.94 mS cm^{-1}). This was similar to another study by Santoro et al.[45] of 2.62 ± 0.04 W m^{-2} that used a different MFC configuration (120 mL MFC, A_{An} = 18 cm^2, A_{Cat} = 2.8 cm^2, $d_{An\text{-}Cat}$ = 4.5 cm, σ=16.4 mS cm^{-1}) and a different Fe-N-C ORR catalyst. Thus, on the basis of the maximum power density alone, the performance of the two systems were quite similar, suggesting that the cathodes performed equally well in the two different MFCs. However, the MFC used by Santoro et al. was designed to have a much larger anode than cathode area (An:Cat projected area ratio of 6.4), so that the anode would not limit power production, while the MFC used by Yang et al. reactor had more similar-sized projected electrode areas (An:Cat = 0.82). Using the EPS analysis, and polarization data corrected for ohmic losses between the working and reference electrodes, the anode area-resistance was R_{An} = 4.30 ± 0.02 mΩ m^2 for the Santoro et al. MFC (Figure 4). This was about four times less than that obtained by Yang et al. (R_{An} = 19 ± 1 mΩ m^2), demonstrating the impact of the different relative electrode sizes on the resistances. The anode experimental potentials were similar, with $E_{An,e0}$ = –281.4 ± 0.2 mV (Santoro et al.) and –268± 7 mV (Yang et al.). The results obtained here for the 70% DL MFCs

(R_{An} = 10.6 ± 0.5 mΩ m^2, $E_{An,e0}$ = –260 ± 3 mV, 70% DL) are also shown in Figure 4 to provide a comparison to these previous two studies.

For the cathodes, the EPS slope analysis revealed that the main differences in the cathode performance was due to the working potentials of the cathodes (y-intercepts), and not their resistances (polarization data slopes). The measured and experimental cathode potentials were $E_{Cat,m0}$ = 557 mV and $E_{Cat,e0}$ = 442 ± 19 mV in the Yang et al. study, compared to lower values of $E_{Cat,m0}$ = 431 ± 2 mV and $E_{Cat,e0}$ =426 ± 3 mV by Santoro et al. The resistances of the cathodes were 23 ± 3 mΩ m^2 for the Yang et al. study, higher than the 16.7 ± 0.4 mΩ m^2 by Santoro et al.

This comparison of the two studies using the EPS analysis demonstrated that electrode performance can be compared even when the MFC architectures are different. Although the power densities were similar, both the anodes and cathodes had different electrochemical characteristics. The experimental cathode potentials in the Yang et al. study were higher, and thus the cathodes had better electrochemical performance that those in the Santoro et al. study. The power densities were only similar due to the lower area resistance of the anodes in the Santoro et al. study (R_{An} =4.3 ± 0.02 mΩ m^2) because this system was optimized to reduce anode limitations by using a much larger anode than the cathode. However, the advantage of the larger anodes was partly nullified by using a larger electrode spacing of 4.5 cm in the Santoro et al., as this produced a total anode and solution resistance of 31 mΩ m^2 compared to the 0.5 cm spacing by Yang et al. (resistance (R_{An} + R_{Ω}) of 26 mΩ m^2). As a result, of these differences, the total internal specific resistances were comparable (49 mΩ m^2 Yang et al.; 48 mΩ m^2 Santoro et al.), resulting in similar maximum power densities.

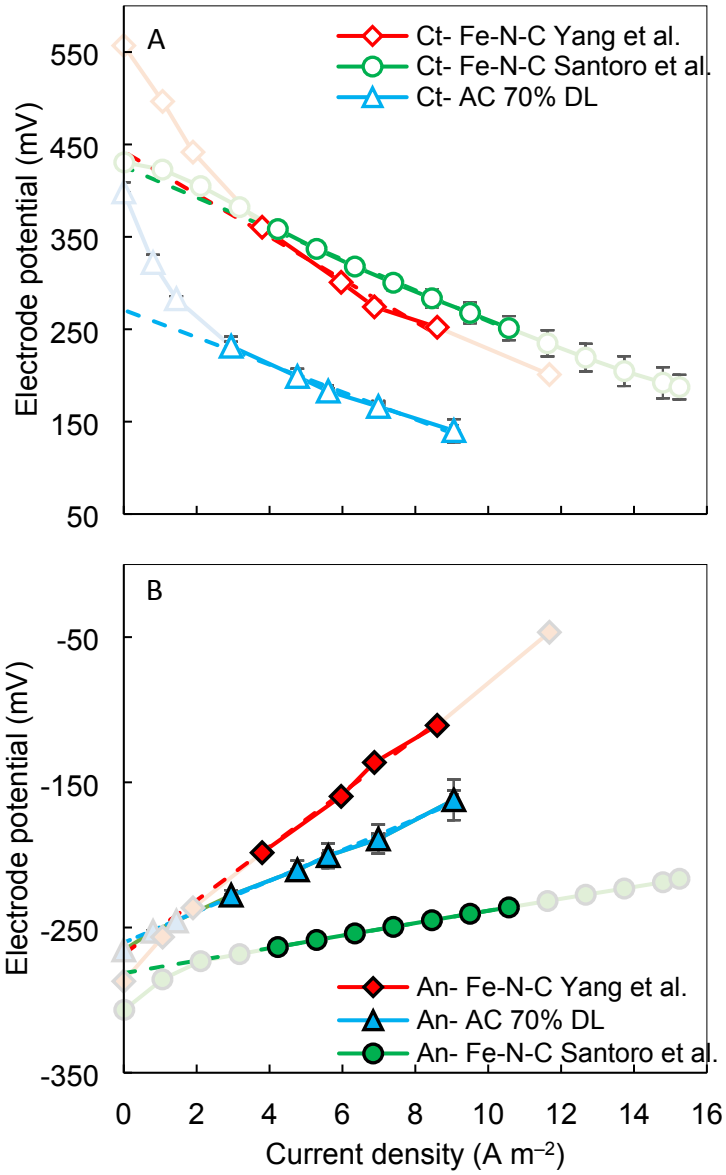

Figure 4. (A) Cathode (Ct) and (B) anode (An) potentials following correction for ohmic resistance using Fe-N-C catalyst developed by Yang et al.[11] and Santoro et al.[45] compared to plain AC cathodes with 70% DL porosities. The results obtained here for the 70% DL MFCs are also shown to provide a comparison of the results of these previous two studies. Anode and cathode potentials not corrected for ohmic losses are reported in the Supporting information (Figure S3). The dashed lines represent the linearization of the data that would be obtained from polarization tests, while the thick solid lines show the linearized portion of the slopes that are used to calculate the anode (R_{An}) and cathode (R_{Cat}) resistances.

Comparison of Pt/C cathodes in 28 mL MFCs. The utility of the EPS analysis was further demonstrated by using it to compare performance of Pt/C cathodes in MFCs for several studies by

409 different research groups (all 28 mL cube reactors, with brush anodes in 50 mM PBS/acetate media)
410 (Figure 5). The average electrode area-based resistances among these studies was R_{cat} = 59 ± 27 mΩ m^2
411 (range 20 mΩ m^2< R_{cat} < 101 mΩ m^2), but the cathode working potentials varied over a much larger
412 range of 242 mV (range 387 mV< $E_{Cat,e0}$ < 145 mV, average of 286 ± 90 mV). The reasons for this large
413 range of working potentials could be due to a lack of proper correction for the ohmic losses between the
414 electrodes[17] or aging of the cathode which reduces performance over time.[9] The potentials presented in
415 figures for the anodes in two of the studies were clearly wrong ($E_{An,e0}$ = –463 mV by Valipour et al.,[46] –
416 475 mV by Meng et al.[47]), as they were 200 mV lower than that possible for acetate oxidation (– 296 mV,
417 eq. 3). In the other five studies,[32,48–51] the anodes had relatively similar anode potentials of $E_{An,e0}$ of –262
418 ± 28 mV and a specific anode resistance of R_{An} = 20 ± 3 mΩ m^2. The reason for the very high anode
419 resistance of R_{An} = 112 mΩ m^2 based on data in Meng et al.[47] is unknown.
420

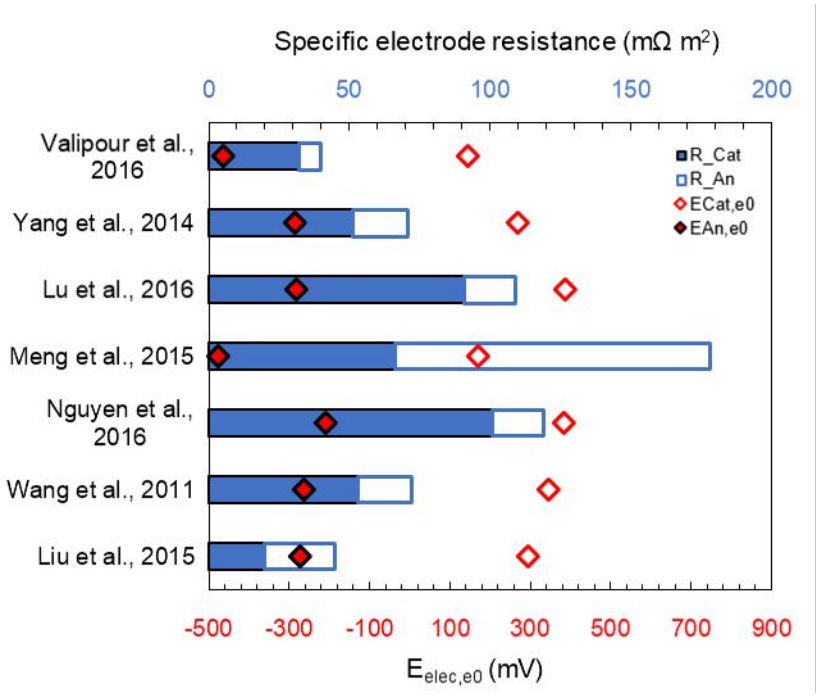

421

422 **Figure 5.** Comparison of Pt/C cathode and brush anode potentials and specific resistances in 28 mL
423 MFCs.
424

Impact of electrode dimensions on area-based resistances using wastewater. Analyzing the slope of similar electrode materials with different dimensions allows to understand how the electrode resistance impacts performance using larger electrodes. In a recent study, we examined power generation using brush anodes and cathodes with projected sizes of 7 cm^2 or 6200 cm^2 in MFCs treating domestic wastewater.[15,52] Although the same materials were used for the electrodes (brush anodes, activated carbon cathodes), the large cathode had a stainless steel frame to hold multiple cathode panels, so the working area was reduced to 4800 cm^2 (Figure S4). The maximum power density decreased from 0.304 ± 0.009 W m^{-2} to 0.101 ± 0.006 W m^{-2} by increasing the electrode size. The experimental cathode potentials were different, with $E_{Cat,e0}$ = 368 ± 8 mV for the large cathode, and $E_{Cat,e0}$ = 265 ± 22 mV (70% DL) for the 7 cm^2 cathode (Figure 6).[15] If the electrode performance remained constant with increases in electrode size, then the area resistances should be constant. However, the large electrode cathode specific resistance was 555 ± 24 mΩ m^2, compared to 66 ± 17 mΩ m^2 for the smaller cathode. Thus, we can directly quantify the cathode performance using the EPS analysis as an area-resistance that increased by 8× using the larger cathode.

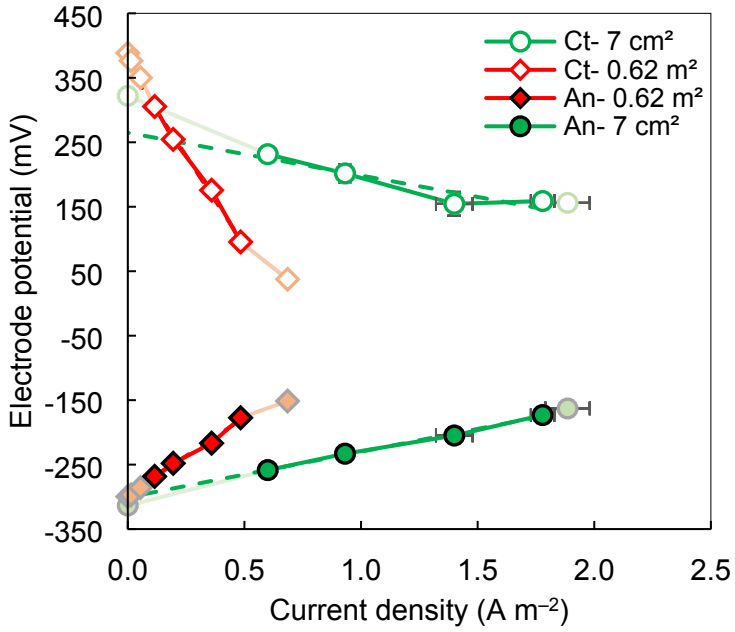

Figure 6. Comparison of anode (An) and cathode (Ct) potentials with projected areas of 7 cm^2 and 0.62 m^2 in wastewater following correction for ohmic resistance. Anode and cathode potentials not corrected for ohmic losses are reported in the Supporting information (Figure S5). The dashed lines represent the linearization of the data that would be obtained from polarization tests, while the thick solid lines show the linearized portion of the slopes that are used to calculate the anode (R_{An}) and cathode (R_{Cat}) resistances.

The anode performance was also impacted by using larger electrodes, but to a lesser extent than the cathodes. The resistance for an array of 22 brush anodes (each 5.1 cm in diameter, and 61 cm long) in the larger MFC was 238 ± 18 mΩ m^2, which was 3× higher than that of the smaller anodes (71 ± 3 mΩ m^2, 2.5 cm in diameter, and 2.5 cm long). The estimated anode potential was $E_{An,e0}$ =–296 ±6 mV, which was similar to that of the small anode ($E_{An,e0}$ =–301 ± 4 mV). The impact of the increase of electrode specific resistance on the sizes of the electrodes have previously only been compared in terms of current or power densities. For example, it was estimated that the electrical power loss could be as much as 47% by increasing the size of a carbon mesh anode from 10 cm^2 to 10000 cm^2 (current density of 3 A m^{-2}), based on only one connection to the electrode.[14] The EPS analysis, however, makes it possible to directly compare the anode or cathode resistances rather than just the overall performance. Overall, for

the large MFC, the cathode resistance was 2.3x that of the anode resistance, and 6.4x larger than the solution resistance, thus, the main resistance in the large MFC was clearly the cathode. This is different from the small chamber MFC where the solution resistance using wastewater was larger than the anode and cathode specific resistances.

Recommendations for future MFC studies. The EPS analysis allows a simple and quantitative comparison of the performance of electrodes or whole cells for a wide range of MFC configurations. The analysis is based on the use of the polarization data near peak power, therefore, no additional electrochemical tests such as EIS or LSVs are needed. However, the analysis requires specific and accurate data for making the calculations which include: the projected areas of both electrodes, the solution conductivity, and the spacing between the reference and working electrodes. Providing solution conductivities is even more important when working with wastewater, which may have different characteristics not only for different locations in the treatment plant, but also at different times of the day. The impact of the solution conductivity on the electrode performance was clearly shown in this study, as the solution specific resistance of the MFCs with PBS (14 mΩ m^2) was 6.2 times lower than that of the MFCs with wastewater (87 mΩ m^2). The polarization tests conducted in wastewater resulted in anode and cathode specific resistances that were 7 times larger in wastewater (30% DL: R_{An} = 78 ± 2 mΩ m^2, R_{Ct} = 78 ± 14 mΩ m^2) than PBS (30% DL R_{An} = 11 ± 1 mΩ m^2, R_{Ct} = 12 ± 5 mΩ m^2).

By using the EPS analysis to determine electrode potentials and area-based resistances, the reasons for the different performance in each configuration can be easily assessed based on electrode potentials and resistances, or possible errors can be identified. For example, while the working potentials and area-based electrode resistances obtained by an EPS analysis of the electrodes were seen to be similar in several studies examined (Figure 5), errors were clearly obvious for two studies where the $E_{An,e0}$ was more negative than that possible based on a thermodynamic calculation.[46,47] If the $E_{An,e0}$ had been

calculated in that study, this error could likely have been avoided as it would have been more obvious that the value was not possible. For the anodes, the area resistances in the studies examined here were fairly similar, and thus the main differences were due to the cathode potentials and area-based resistances. The EPS analysis makes it possible to quantify these individual resistances, when ohmic resistances are separately reported and electrode potentials are corrected for ohmic drops between the reference and working electrodes.[17] Thus, the use of this method enables an easier and more direct comparison of performance of these different electrode materials based on the quantitative analysis of components, rather than the overall power density.

ASSOCIATED CONTENT

Supporting Information.

Three figures showing anode and cathode potentials not corrected for the solution conductivity, one figure showing the impact of the current density range on the electrode resistance and the experimental potentials and a figure showing the air and the solution side of a scaled-up cathode. This material is available free of charge via the Internet at http://pubs.acs.org.

AUTHOR INFORMATION

Corresponding Author

*E-mail: blogan@psu.edu. Phone: +1-814-863-7908, Fax: +1 814 863-7304.

ORCHID

Bruce E. Logan: 0000-0001-7478-8070

Ruggero Rossi: 0000-0002-3807-3980

Notes

The authors declare no competing financial interest.

Acknowledgments

The research was supported by funds provided by the Environmental Security Technology Certification Program via cooperative research agreement W9132T-16-2-0014 through the US Army Engineer Research and Development Center.

References

(1) Logan, B. E.; Hamelers, B.; Rozendal, R.; Schröder, U.; Keller, J.; Freguia, S.; Aelterman, P.; Verstraete, W.; Rabaey, K. Microbial Fuel Cells: Methodology and Technology. *Environ. Sci. Technol.* **2006**, *40* (17), 5181–5192.

(2) Logan, B. E.; Wallack, M. J.; Kim, K. Y.; He, W.; Feng, Y.; Saikaly, P. E. Assessment of Microbial Fuel Cell Configurations and Power Densities. *Environ. Sci. Technol. Lett.* **2015**,

519 *2* (8), 206–214.
520 (3) Lovley, D. R. Bug Juice: Harvesting Electricity with Microorganisms. *Nat. Rev. Microbiol.*
521 **2006**, *4* (7), 497–508.
522 (4) Li, W.-W.; Yu, H.-Q.; He, Z. Towards Sustainable Wastewater Treatment by Using
523 Microbial Fuel Cells-Centered Technologies. *Energy Environ. Sci.* **2013**, *7* (3), 911–924.
524 (5) Logan, B.; Cheng, S.; Watson, V.; Estadt, G. Graphite Fiber Brush Anodes for Increased
525 Power Production in Air-Cathode Microbial Fuel Cells. *Environ. Sci. Technol.* **2007**, *41* (9),
526 3341–3346.
527 (6) Cheng, S.; Logan, B. E. Ammonia Treatment of Carbon Cloth Anodes to Enhance Power
528 Generation of Microbial Fuel Cells. *Electrochem. commun.* **2007**, *9* (3), 492–496.
529 (7) Santoro, C.; Arbizzani, C.; Erable, B.; Ieropoulos, I. Microbial Fuel Cells: From
530 Fundamentals to Applications. A Review. *J. Power Sources* **2017**, *356*, 225–244.
531 (8) Zhang, F.; Yuan, S. J.; Li, W. W.; Chen, J. J.; Ko, C. C.; Yu, H. Q. WO_3 Nanorods-Modified
532 Carbon Electrode for Sustained Electron Uptake from Shewanella oneidensis MR-1 with
533 Suppressed Biofilm Formation. *Electrochim. Acta* **2015**, *152*, 1–5.
534 (9) Yang, W.; Kim, K. Y.; Saikaly, P. E.; Logan, B. E. The Impact of New Cathode Materials
535 Relative to Baseline Performance of Microbial Fuel Cells All with the Same Architecture
536 and Solution Chemistry. *Energy Environ. Sci.* **2017**, *10* (5), 1025–1033.
537 (10) Pant, D.; Van Bogaert, G.; De Smet, M.; Diels, L.; Vanbroekhoven, K. Use of Novel
538 Permeable Membrane and Air Cathodes in Acetate Microbial Fuel Cells. *Electrochim.*
539 *Acta* **2010**, *55* (26), 7710–7716.
540 (11) Yang, W.; Logan, B. E. Immobilization of a Metal – Nitrogen – Carbon Catalyst on
541 Activated Carbon with Enhanced Cathode Performance in Microbial Fuel Cells.
542 *ChemSusChem* **2016**, *9*, 2226–2232.
543 (12) Zhang, X.; Pant, D.; Zhang, F.; Liu, J.; He, W.; Logan, B. E. Long-Term Performance of
544 Chemically and Physically Modified Activated Carbons in Air Cathodes of Microbial Fuel
545 Cells. *ChemElectroChem* **2014**, *1* (11), 1859–1866.
546 (13) Dewan, A.; Beyenal, H.; Lewandowski, Z. Scaling up Microbial Fuel Cells. *Environ. Sci.*
547 *Technol.* **2008**, *42* (20), 7643–7648.
548 (14) Cheng, S.; Ye, Y.; Ding, W.; Pan, B. Enhancing Power Generation of Scale-up Microbial
549 Fuel Cells by Optimizing the Leading-out Terminal of Anode. *J. Power Sources* **2014**, *248*,
550 631–638.
551 (15) Rossi, R.; Jones, D.; Myung, J.; Zikmund, E.; Yang, W.; Alvarez, Y.; Pant, D.; Evans, P. J.;
552 Page, M. A.; Cropek, D. M.; Logan, B. E. Evaluating a Multi-Panel Air Cathode through
553 Electrochemical and Biotic Tests. *Water Res.* **2019**, *148*, 51–59.
554 (16) Fan, Y.; Sharbrough, E.; Liu, H. Quantification of the Internal Resistance Distribution of
555 Microbial Fuel Cells Quantification of the Internal Resistance Distribution of Microbial
556 Fuel Cells. *Environ. Sci. Technol.* **2008**, *42* (21), 8101–8107.
557 (17) Logan, B. E.; Zikmund, E.; Yang, W.; Rossi, R.; Kim, K.-Y.; Saikaly, P. E.; Zhang, F. Impact of
558 Ohmic Resistance on Measured Electrode Potentials and Maximum Power Production in
559 Microbial Fuel Cells. *Environ. Sci. Technol.* **2018**, *52*, 8977–8985.
560 (18) Logan, B. E. Scaling up Microbial Fuel Cells and Other Bioelectrochemical Systems. *Appl.*
561 *Microbiol. Biotechnol.* **2010**, *85* (6), 1665–1671.
562 (19) Ribot-Llobet, E.; Nam, J. Y.; Tokash, J. C.; Guisasola, A.; Logan, B. E. Assessment of Four

563 Different Cathode Materials at Different Initial pHs Using Unbuffered Catholytes in
564 Microbial Electrolysis Cells. *Int. J. Hydrogen Energy* **2013**, *38* (7), 2951–2956.
565 (20) Zhang, Y.; Merrill, M. D.; Logan, B. E. The Use and Optimization of Stainless Steel Mesh
566 Cathodes in Microbial Electrolysis Cells. *Int. J. Hydrogen Energy* **2010**, *35* (21), 12020–
567 12028.
568 (21) Aulenta, F.; Catapano, L.; Snip, L.; Villano, M.; Majone, M. Linking Bacterial Metabolism
569 to Graphite Cathodes: Electrochemical Insights into the H2-Producing Capability of
570 Desulfovibrio Sp. *ChemSusChem* **2012**, *5* (6), 1080–1085.
571 (22) Velasquez-Orta, S. B.; Curtis, T. P.; Logan, B. E. Energy from Algae Using Microbial Fuel
572 Cells. *Biotechnol. Bioeng.* **2009**, *103* (6), 1068–1076.
573 (23) Yan, H.; Yates, M. D.; Regan, J. M. Effects of Constant or Dynamic Low Anode Potentials
574 on Microbial Community Development in Bioelectrochemical Systems. *Appl. Microbiol.*
575 *Biotechnol.* **2015**, *99* (21), 9319–9329.
576 (24) Jung, S.; Regan, J. M. Influence of External Resistance on Electrogenesis,
577 Methanogenesis, and Anode Prokaryotic Communities in Microbial Fuel Cells. *Appl.*
578 *Environ. Microbiol.* **2011**, *77* (2), 564–571.
579 (25) Lewis, A. J.; Borole, A. P. Adapting Microbial Communities to Low Anode Potentials
580 Improves Performance of MECs at Negative Potentials. *Electrochim. Acta* **2017**, *254*, 79–
581 88.
582 (26) Zhang, F.; Liu, J.; Ivanov, I.; Hatzell, M. C.; Yang, W.; Ahn, Y.; Logan, B. E. Reference and
583 Counter Electrode Positions Affect Electrochemical Characterization of Bioanodes in
584 Different Bioelectrochemical Systems. *Biotechnol. Bioeng.* **2014**, *111* (10), 1931–1939.
585 (27) Liang, P.; Huang, X.; Fan, M. Z.; Cao, X. X.; Wang, C. Composition and Distribution of
586 Internal Resistance in Three Types of Microbial Fuel Cells. *Appl. Microbiol. Biotechnol.*
587 **2007**, *77* (3), 551–558.
588 (28) Sleutels, T. H. J. A.; Hamelers, H. V. M.; Rozendal, R. A.; Buisman, C. J. N. Ion Transport
589 Resistance in Microbial Electrolysis Cells with Anion and Cation Exchange Membranes.
590 *Int. J. Hydrogen Energy* **2009**, *34* (9), 3612–3620.
591 (29) Wen, Q.; Wu, Y.; Cao, D.; Zhao, L.; Sun, Q. Electricity Generation and Modeling of
592 Microbial Fuel Cell from Continuous Beer Brewery Wastewater. *Bioresour. Technol.* **2009**,
593 *100* (18), 4171–4175.
594 (30) Rismani-Yazdi, H.; Carver, S. M.; Christy, A. D.; Tuovinen, O. H. Cathodic Limitations in
595 Microbial Fuel Cells: An Overview. *J. Power Sources* **2008**, *180* (2), 683–694.
596 (31) Feng, C.; Li, F.; Liu, H.; Lang, X.; Fan, S. A Dual-Chamber Microbial Fuel Cell with
597 Conductive Film-Modified Anode and Cathode and Its Application for the Neutral Electro-
598 Fenton Process. *Electrochim. Acta* **2010**, *55* (6), 2048–2054.
599 (32) Nguyen, M. T.; Mecheri, B.; Iannaci, A.; D'Epifanio, A.; Licoccia, S. Iron/Polyindole-Based
600 Electrocatalysts to Enhance Oxygen Reduction in Microbial Fuel Cells. *Electrochim. Acta*
601 **2016**, *190*, 388–395.
602 (33) Watson, V. J.; Logan, B. E. Analysis of Polarization Methods for Elimination of Power
603 Overshoot in Microbial Fuel Cells. *Electrochem. commun.* **2011**, *13* (1), 54–56.
604 (34) Zhu, X.; Tokash, J. C.; Hong, Y.; Logan, B. E. Controlling the Occurrence of Power
605 Overshoot by Adapting Microbial Fuel Cells to High Anode Potentials. *Bioelectrochemistry*
606 **2013**, *90*, 30–35.

(35) Shao, Z.; Halle, S. M. A High-Performance Cathode for the next Generation of Solid-Oxide Fuel Cells. *Nature* **2004**, *431* (7005), 170–173.
(36) Popat, S. C.; Ki, D.; Rittmann, B. E.; Torres, C. I. Importance of OH^- Transport from Cathodes in Microbial Fuel Cells. *ChemSusChem* **2012**, *5* (6), 1071–1079.
(37) Rojas-Carbonell, S.; Artyushkova, K.; Serov, A.; Santoro, C.; Matanovic, I.; Atanassov, P. Effect of pH on the Activity of Platinum Group Metal-Free Catalysts in Oxygen Reduction Reaction. *ACS Catal.* **2018**, *8* (4), 3041–3053.
(38) Watson, V. J.; Nieto Delgado, C.; Logan, B. E. Influence of Chemical and Physical Properties of Activated Carbon Powders on Oxygen Reduction and Microbial Fuel Cell Performance. *Environ. Sci. Technol.* **2013**, 130603162645003.
(39) Santoro, C.; Kodali, M.; Kabir, S.; Soavi, F.; Serov, A.; Atanassov, P. Three-Dimensional Graphene Nanosheets as Cathode Catalysts in Standard and Supercapacitive Microbial Fuel Cell. *J. Power Sources* **2017**, *356*, 371–380.
(40) Min, B.; Cheng, S.; Logan, B. E. Electricity Generation Using Membrane and Salt Bridge Microbial Fuel Cells. *Water Res.* **2005**, *39* (9), 1675–1686.
(41) Feng, Y.; Yang, Q.; Wang, X.; Logan, B. E. Treatment of Carbon Fiber Brush Anodes for Improving Power Generation in Air-Cathode Microbial Fuel Cells. *J. Power Sources* **2010**, *195* (7), 1841–1844.
(42) Zhang, F.; Pant, D.; Logan, B. E. Long-Term Performance of Activated Carbon Air Cathodes with Different Diffusion Layer Porosities in Microbial Fuel Cells. *Biosens. Bioelectron.* **2011**, *30* (1), 49–55.
(43) Lovley, D. R.; Phillips, E. J. P. Novel Mode of Microbial Energy Metabolism: Organic Carbon Oxidation Coupled to Dissimilatory Reduction of Iron or Manganese. *Appl. Envir. Microbiol.* **1988**, *54* (6), 1472–1480.
(44) Rossi, R.; Yang, W.; Setti, L.; Logan, B. E. Assessment of a Metal – Organic Framework Catalyst in Air Cathode Microbial Fuel Cells over Time with Different Buffers and Solutions. *Bioresour. Technol.* **2017**, *233*, 399–405.
(45) Santoro, C.; Kodali, M.; Herrera, S.; Serov, A.; Ieropoulos, I.; Atanassov, P. Power Generation in Microbial Fuel Cells Using Platinum Group Metal-Free Cathode Catalyst: Effect of the Catalyst Loading on Performance and Costs. *J. Power Sources* **2018**, *378*, 169–175.
(46) Valipour, A.; Ayyaru, S.; Ahn, Y. Application of Graphene-Based Nanomaterials as Novel Cathode Catalysts for Improving Power Generation in Single Chamber Microbial Fuel Cells. *J. Power Sources* **2016**, *327*, 548–556.
(47) Meng, K.; Liu, Q.; Huang, Y.; Wang, Y. Facile Synthesis of Nitrogen and Fluorine Co-Doped Carbon Materials as Efficient Electrocatalysts for Oxygen Reduction Reactions in Air-Cathode Microbial Fuel Cells. *J. Mater. Chem. A* **2015**, *3* (13), 6873–6877.
(48) Yang, W.; Zhang, F.; He, W.; Liu, J.; Hickner, M. A.; Logan, B. E. Poly(vinylidene Fluoride-Co-Hexafluoropropylene) Phase Inversion Coating as a Diffusion Layer to Enhance the Cathode Performance in Microbial Fuel Cells. *J. Power Sources* **2014**, *269*, 379–384.
(49) Lu, G.; Zhu, Y.; Lu, L.; Xu, K.; Wang, H.; Jin, Y.; Jason Ren, Z.; Liu, Z.; Zhang, W. Iron-Rich Nanoparticle Encapsulated, Nitrogen Doped Porous Carbon Materials as Efficient Cathode Electrocatalyst for Microbial Fuel Cells. *J. Power Sources* **2016**, *315*, 302–307.
(50) Wang, L.; Liang, P.; Zhang, J.; Huang, X. Activity and Stability of Pyrolyzed Iron

651 Ethylenediaminetetraacetic Acid as Cathode Catalyst in Microbial Fuel Cells. *Bioresour.*
652 *Technol.* **2011**, *102* (8), 5093–5097.
653 (51) Liu, Q.; Zhou, Y.; Chen, S.; Wang, Z.; Hou, H.; Zhao, F. Cellulose-Derived Nitrogen and
654 Phosphorus Dual-Doped Carbon as High Performance Oxygen Reduction Catalyst in
655 Microbial Fuel Cell. *J. Power Sources* **2015**, *273*, 1189–1193.
656 (52) Rossi, R.; Evans, P. J.; Logan, B. E. Impact of Flow Recirculation and Anode Dimensions on
657 Performance of a Large Scale Microbial Fuel Cell. *J. Power Sources* **2019**, *412*, 294–300.
658

659 **Table of Contents (TOC)/Abstract Art**

660

661

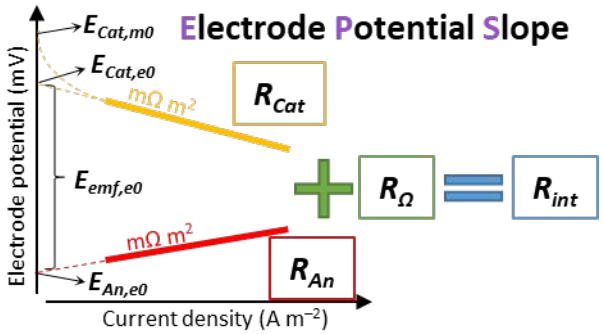

662

663

664

665